Research Article | Vol. 28, No. 12 / 8 June 2020 / Optics Express 18180
Optics EXPRESS

Dual-band single-pixel telescope

YIWEI ZHANG,* GRAHAM M. GIBSON, MATTHEW P. EDGAR, GILES HAMMOND, AND MILES J. PADGETT

SUPA, School of Physics and Astronomy, University of Glasgow, Glasgow, G12 8QQ, UK
*ewayzhang@gmail.com

Abstract: Single-pixel imaging systems can obtain images from a wide range of wavelengths at low-cost compared to those using conventional multi-pixel, focal-plane array sensors, especially at wavelengths outside the visible spectrum. The ability to sense short-wave infrared radiation with single-pixel techniques extends imaging capability to adverse weather conditions and environments, such as fog, haze, or night time. In this work, we demonstrate a dual-band single-pixel telescope for imaging at both visible (VIS) and short-wave infrared (SWIR) spectral regions simultaneously under some of these outdoor weather conditions. At 64×64 pixel-resolution, our system has achieved continuous VIS and SWIR imaging of various objects at a frame rate up to 2.4 Hz. Visual and contrast comparison between the reconstructed VIS and SWIR images emphasizes the significant contribution of infrared observation using the single-pixel technique. The single-pixel telescope provides an alternative cost-effective imaging solution for synchronized dual-waveband optical applications.

1. Introduction

Single-pixel imaging is an alternative choice to the use of focal plane array detectors. Instead of gaining the spatial information from a detector array situated in the focal-plane of a camera, single-pixel imaging [1–5] retrieves the spatial information of a scene from a predefined sampling mask set. A single-pixel imaging system generally consists of a single detector that simply records the total back-scattered light intensity from a scene and a spatial light modulator (SLM) which is used to either project structured light patterns onto a scene, named structured illumination, or structure the detection of the back-scattered intensities from the field of view, termed structured detection [1,6]. Different SLM technologies can be used in single-pixel imaging, depending on the application. In computational imaging systems, a digital micromirror device (DMD) is a most commonly used SLM due to its superior modulation rate, compared to those based upon liquid crystal technology, and its broadband wavelength response.

To obtain a full image of a scene using a single-pixel technique in principle requires the same amount of sampling as the number of desired pixels in the image. In practice this number can be reduced using compressed sensing techniques which will be considered later.

Mathematically, the measurement of single-pixel light intensity is equivalent to the inner product between the patterns and the object. Given a sequence of N-element orthonormal pattern pairs $P_{i,m}$ (i is the pixel number and $i \in [1, \ N]$, m is the pattern sequence number), the corresponding differential signal is $S_{m,n}$. For a pattern sequence the n^{th} image estimate of the object $I_{(x,y),\,n}$, reformatted as a column vector $I_{i,\,n}$, can be represented by the mathematical expression

$$I_{i,n} = \frac{1}{n} \sum_{m=1}^{n} S_{m,n} P_{i,m} \tag{1}$$

#392522 https://doi.org/10.1364/OE.392522
Journal © 2020 Received 13 Mar 2020; revised 17 May 2020; accepted 19 May 2020; published 3 Jun 2020

Optics EXPRESS

where $n = N$ is the least amount of sampling required to fully, and unambiguously, reconstruct a single image of an entire scene under the condition that each pattern P_m in the sampling set is orthogonal to all others.

Over the last decade, single-pixel techniques have been utilized in numerous challenging frameworks, for instance, photon counting regimes [7,8], spatial entanglement detection [9,10], and multi-dimensional imaging [11–13]. Besides performing in the visible spectrum, single-pixel imaging has demonstrated its viability in exotic regions of the electromagnetic spectrum, such as terahertz [2,14–16] and infrared [17–21], where conventional imaging techniques face difficulties in both practicality and cost. Recent reviews of single-pixel imaging, including its relationship to computational ghost imaging, are provided by Edgar et al. [6] and Sun and Zhang [22].

In this work, we demonstrate a dual-band single-pixel telescope, capable of performing real-time multispectral images in both visible (VIS) and short-wave infrared (SWIR) bands simultaneously. Instead of collecting only the light reflected from the DMD pixels in the "on" state, as in conventional single-pixel systems, we have created double optical paths with a differential signal acquisition approach to also take advantage of the light reflected from the DMD pixels in the "off" state. This differential approach allows two images with perfect overlap to be reconstructed and importantly can be based on measurements using two different detector types. It is important to note that the broad wavelength response of the DMD is compatible with the combined wavelength response of the two detectors. We apply this system to imaging different objects including distant ground-based structures in various weather conditions. Our single-pixel telescope provides an alternative cost-effective method for multispectral imaging applications.

2. Experimental setup

A diagram of the dual-band single-pixel telescope setup is shown in Fig. 1(c). The imaging system is based on a Maksutov-Newtonian telescope (Sky-Watcher BK MN190 EQ6 SynScan) with a focal length of one meter to which is mounted our single-pixel camera. The camera comprises a DMD (ViALUX DLP V-7001) with a binary pattern switching rate up to 22.7 kHz. The DMD has an active 1024×768 mirror array area of 14.0 mm x 10.5 mm, each of which tilts +12 degrees or −12 degrees with respect to the DMD surface forming binary patterns, as illustrated in Fig. 1(a). In our system, we use a side length of 7mm of the DMD central square mirror array area to display the patterns. Two single-pixel detectors, each with a different spectral response, are attached to opposite sides of the DMD. Each detector measures light reflected from the DMD at $\pm 24^\circ$ (i.e. $2 \times 12^\circ$) as shown in Fig. 1(b). This allows light reflected from the DMD to be collected from both optical paths simultaneously rather than wasting half of the signal. As the variation in the signals received from those two optical paths are inverse to each other, here we display each pattern followed by its contrast-reversed inverse and adopt the differential signal intensity value for each corresponding mask [23]. Concerning the measurement patterns, a commonly-used Hadamard-coded pattern set [6], in which each pattern is orthogonal to the rest, is employed in structured detection to allow perfect image reconstruction with the number of patterns equivalent to the number of pixels in the image.

One of the detectors in the system is a multi-alkali amplified photomultiplier tube (Thorlabs PMM02) for light signals ranging from 300 nm to 800 nm wavelength (visible wavelength range). A control circuit is used to set the gain of the detector. The other detector is an InGaAs switchable gain detector (Thorlabs PDA20CS) for light signals ranging from 800 nm to 1800 nm wavelength (SWIR wavelength range). Since both detectors receive signals at the same time, it enables our system, as shown in Fig. 2, to perform dual VIS/SWIR waveband imaging simultaneously with perfect pixel registration between the two reconstructed images.

Optics EXPRESS

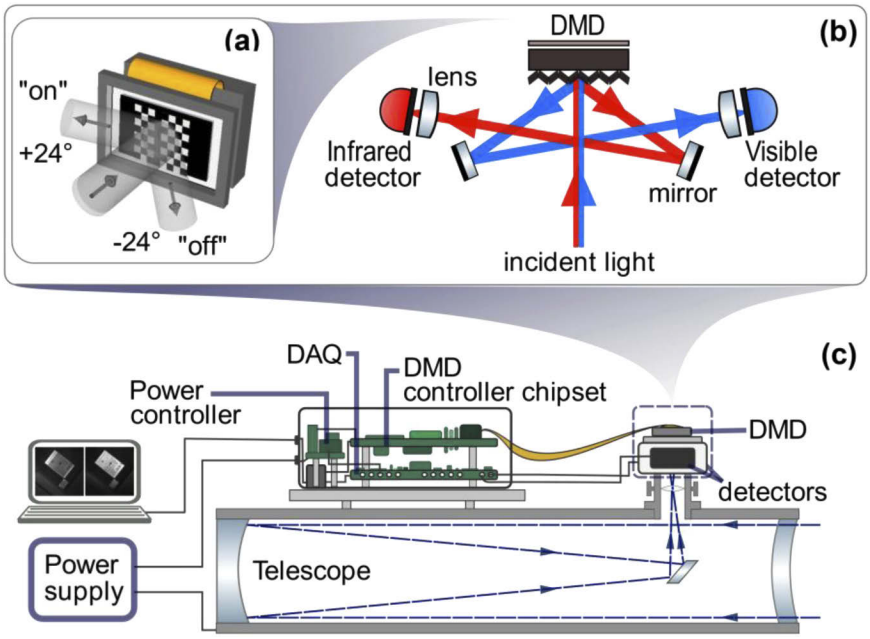

Fig. 1. An illustration of the DMD and system diagram. (a) Schematic of the DMD operation. Each micro-mirror on an illuminated DMD tilts at either + 12 or -12 degrees to represent an "on" or "off" state. (b) The propagation path of light from the DMD to two detectors. Two mirrors reflect light from the DMD towards separate VIS and IR detectors. (c) Experimental setup. A DMD is positioned near the focal plane at the top side port of the telescope tube. A detector is installed on both sides of the DMD with a lens in front of each detector to collect light. An external battery is attached to supply the power for both detectors and the DMD. A laptop is connected to the DMD board to load the pattern sequence and perform image reconstruction.

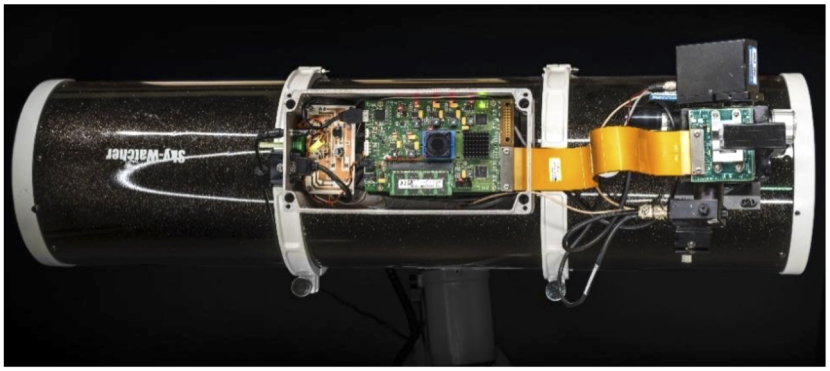

Fig. 2. A top view of the dual-band single-pixel telescope system.

Optics EXPRESS

3. Differential signal processing

The Hadamard basis patterns employed in the structured detection are generated following the Walsh matrices [24–26] of a core matrix of order 2, where

$$H_2 = \begin{bmatrix} 1 & 1 \\ 1 & -1 \end{bmatrix}, \tag{2}$$

$$H_{2^k} = \begin{bmatrix} H_{2^{k-1}} & H_{2^{k-1}} \\ H_{2^{k-1}} & -H_{2^{k-1}} \end{bmatrix}. \tag{3}$$

Each matrix constructed following this approach is orthogonal, symmetric and involutive, which greatly simplifies the complexity of performing matrix computations and reduces the measurement redundancy.

In a traditional Hadamard single-pixel imaging scheme, the DMD displays a white (+1) or black (0) pattern corresponding to the value + 1 or -1 of H_{2^k} for each coordinate (x, y) in the plane. The mean signal value detected under each pattern is collected to reconstruct the 2D image following Eq. (1).

For this single-pixel telescope system, a differential signal acquisition approach is adopted [6,23]. Instead of mapping the signals from DMD patterns directly with the Walsh matrices, we project each pattern followed by its contrast-reversed inverse, where the mirrors in the 'on' state are set to 'off' and vice versa. We then take the differential values between these patterns and correlate with the original Hadamard derived patterns. Under this approach, the effective elements of each DMD pattern becomes + 1 and -1 rather than + 1 and 0, hence provides a better fit with the Walsh matrices and hence more accurate reconstruction. In addition, the background signal noise is noticeably reduced with the differential scheme comparing to the ones using non-paired patterns, especially with illumination noise, which comes at some cost of overall illumination efficiency.

4. Results

The performance of the single-pixel telescope is analyzed through imaging a range of static and dynamic scenes. All images captured were taken on sunny days with either a blue sky or some clouds in the background at various distances. A mirror array of 512×512 in the central area of the DMD was used to structure the detected light with paired patterns derived from the Walsh matrices. Due to the resolution of the reconstructed images being lower than the number of available micromirrors, the patterns had to be scaled up to fill the selected DMD area.

4.1. Image reconstruction of static objects under artificial fog

In one experiment, we used the dual-band single-pixel telescope to acquire images of some static object with a theatrical smoke machine blowing water based white fog in front of the telescope.

In Fig. 3(a), a sculpture on the main building tower at the University of Glasgow, as highlighted by a purple box, was captured while the smoke machine was running periodically. The distance between the sculpture and the telescope was ~150 meters based on Google Maps, as shown in Fig. 3(b), and the smoke machine was placed ~2 meters in front of the telescope. At the time the single-pixel images were acquired there was no cloud cover and the sky behind the sculpture was blue due to the fact that blue light is scattered more than the rest of the visible range by the tiny molecules of the air in the Earth's atmosphere. Hence the background in the SWIR images was dark while the background in the VIS images was bright. Figure 3(c) presents a sample of VIS and SWIR frames reconstructed at a resolution of 64×64 at a frame rate of ~2.4 Hz, where it is

Optics EXPRESS

observed that in some of the frames the sculpture is completely obscured by the fog in the VIS channel while it remains visible in the SWIR channel.

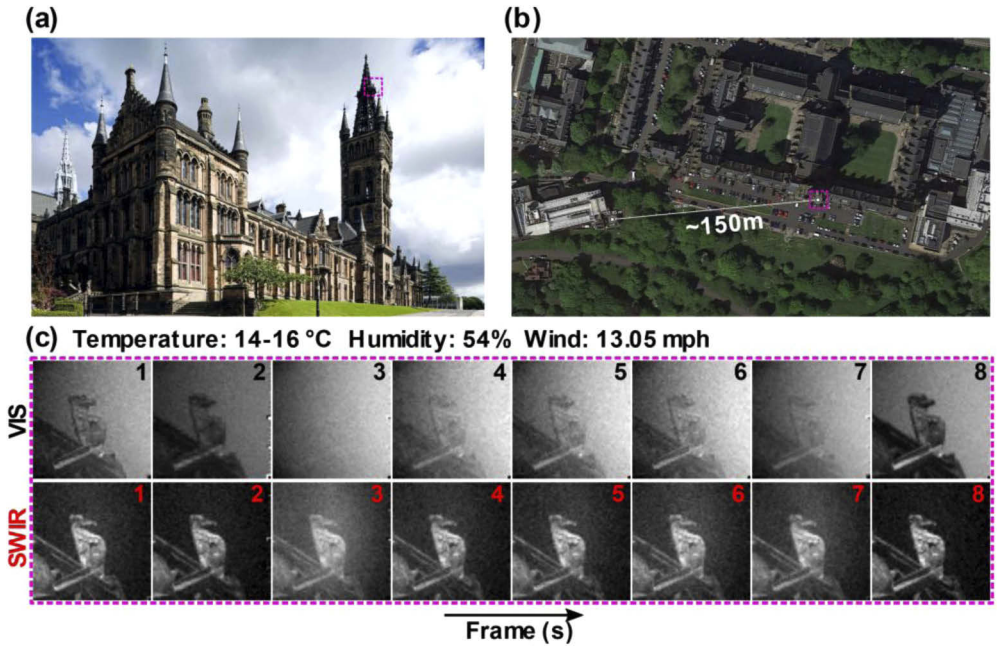

Fig. 3. Imaging results of a selected sculpture on the main building tower at the University of Glasgow. (a) A visual image of the main building taken by a digital single-lens reflex (DSLR) camera. (b) The distance between the tower and the single-pixel telescope is ~150 m. (c) Real-time reconstructed VIS and SWIR images of the sculpture at 64×64 resolution with artificial fog blowing from a theatre smoke machine in front of the telescope.

4.2. Image reconstruction of dynamic scenes under natural weather conditions

In a separate experiment, we analyzed the performance of the dual-band telescope system by imaging dynamic scenes under natural weather conditions.

In Fig. 4, some wind turbines from the Glasgow Whitelee windfarm were captured at a distance of ~18 km. Figures 4(c), 4(d), and 4(e) present samples of VIS and SWIR frames reconstructed at 64×64 pixel resolution under three weather conditions. We could observe that for this scene, the SWIR channel gives more details of the wind turbines compared to the VIS one under natural haze condition, as shown in Fig. 4(c). By utilizing a set of VIS and SWIR frames, an estimate of the contrast in the scene was calculated, as shown in Fig. 5. Under each weather condition, a set of 8 frames from both channels was combined to improve the signal to noise ratio. A similar region from some static part of the wind turbines under each weather condition (shown as a yellow box in Fig. 5) was chosen and the contrasts of each horizontal row in the region from the averaged VIS and SWIR images were compared. The results show that the SWIR images have a better contrast than the VIS images in all of the three weather conditions.

Although single pixel cameras have a number of technological advantages over focal plane arrays, they also have limitations. Perhaps the main limitation relates to their inherently low sensitivity in low light conditions. This limitation arises from the fact that whereas for a focal plane array the dynamic range of the image is reflected in the signals recorded by each of the pixels in the array, however, for a single-pixel camera the image information is contained only in the pattern-to-pattern variation of the signal which is only a fraction of the average signal.

Optics EXPRESS

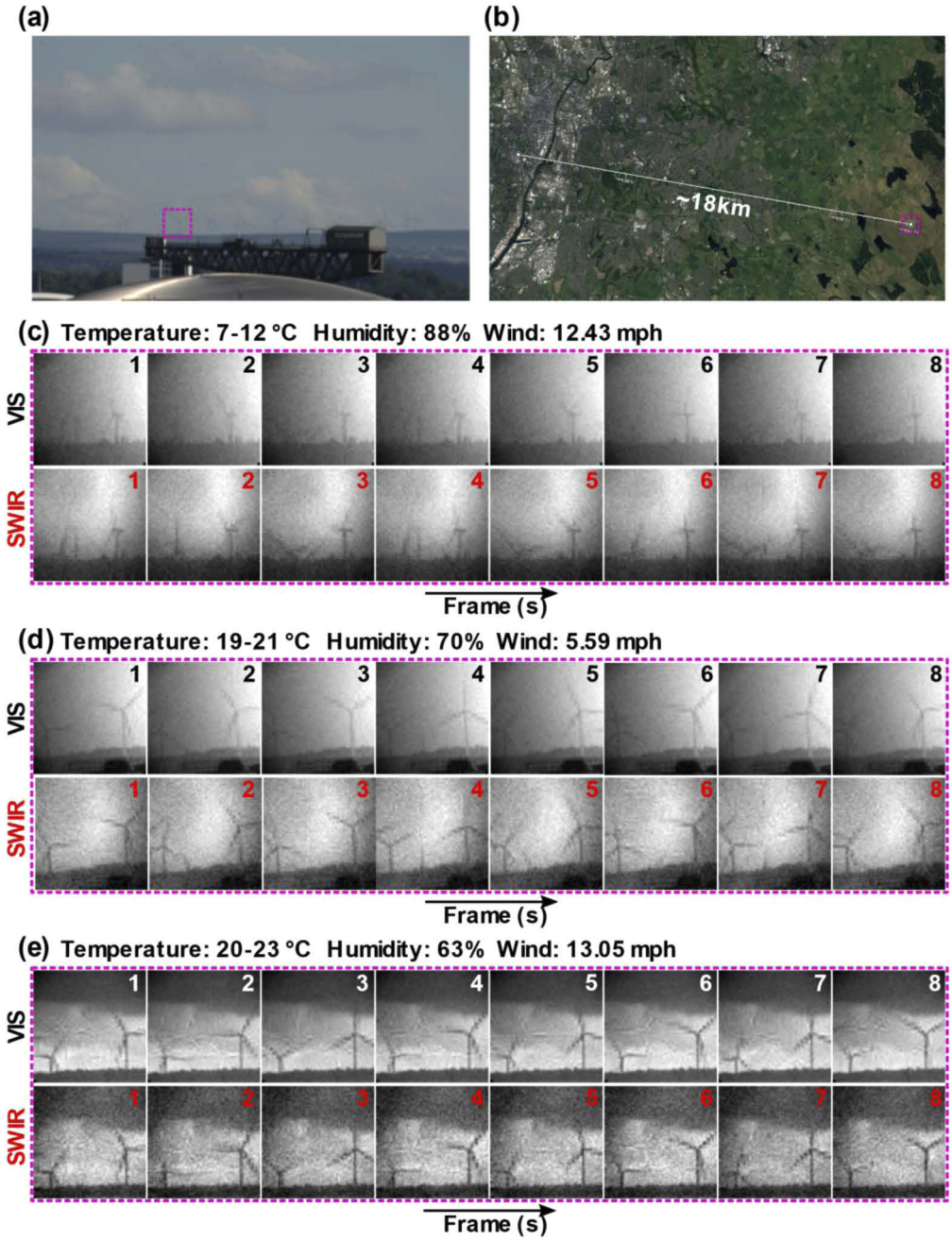

Fig. 4. Imaging results of some wind turbines from the Whitelee windfarm in Glasgow. (a) An image looking towards the windfarm, taken using a DSLR camera, where the location of the turbines is indicated by the purple region. (b) The distance between the wind turbines and telescope is ~18 km. (c, d, e) Reconstructed VIS and SWIR images at 64×64 under weather conditions of (c) temperature 7-12 °C, humidity 88%, wind speed 12.43 mph, (d) temperature 19-21 °C, humidity 70%, wind speed 5.59 mph, and (e) temperature 20-23 °C, humidity 63%, wind speed 13.05 mph.

Optics EXPRESS

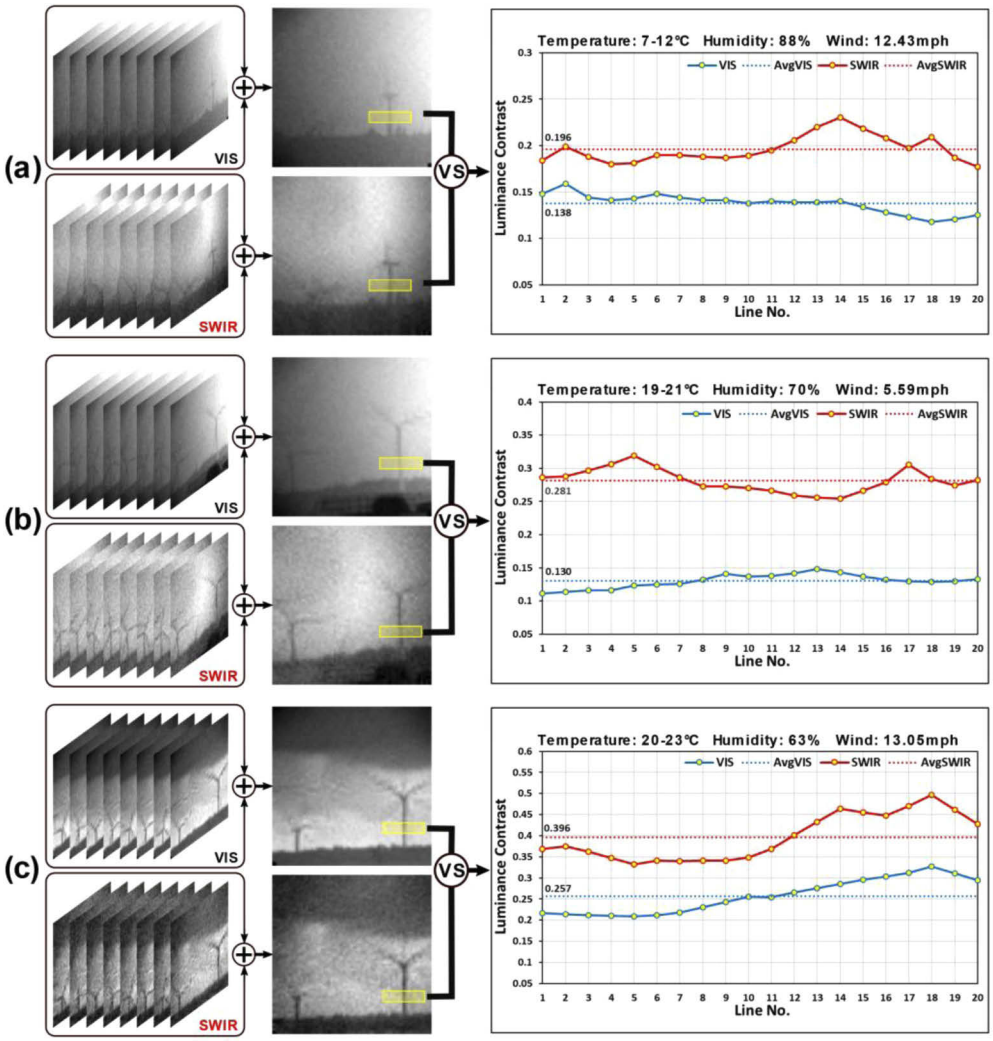

Fig. 5. Luminance contrast comparison. Under each weather condition (a-c), a set of frames from each channel were combined to compose an image with improved signal to noise ratio. The luminance contrast of each row from a same yellow marked region between the VIS and SWIR images were compared.

Optics EXPRESS

Hence the single-pixel configuration requires more light to ensure that the image information exceeds both the noise floor of the detector and the intensity noise associated with the light source (ultimately set by the shot noise). The precise relationship between the two approaches depends upon the detailed nature of the patterns and image scenes and the desired resolution.

This being said it is therefore useful to test our imaging system in a known low-light application. We therefore use our single-pixel telescope to capture images of the moon at night. Figure 6 shows both VIS and SWIR images of the moon taken under clear sky condition at night time. We demonstrate that useful images can be obtained using a 1m focal length and f-number of 5.3, at resolution 64×64 and frame rate ~1.2 Hz. As expected, the achievable frame rate is lower for these low-light conditions than for the daylight conditions of the previous experiments. By comparison, a conventional DSLR camera also operating at an f-number of 5.6 and an ISO film speed of 100 would typically require a shutter speed of 1/500th second [27], albeit in the visible region of the spectrum. The lower sensitivity of a single-pixel camera, compared to a state-of-the-art focal plane array stems from the single-pixel data being of low contrast due to the practical correlations between the object and the measurement patterns [28]. Hence the technical simplicity of the single pixel approach has a disadvantage of inherently reduced sensitivity. Due to the constant motion of the moon, increasing the resolution would introduce extra noise in the images, unless tracking techniques are used.

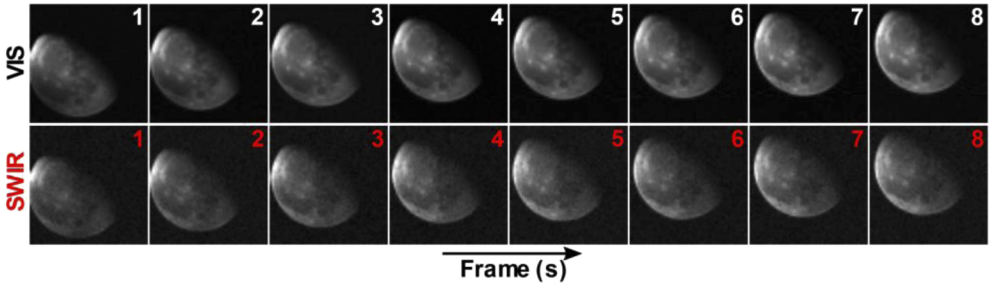

Fig. 6. Imaging results of the moon under clear sky condition at night time. Samples of reconstructed VIS and SWIR images of the moon at 64×64 with a frame rate of ~1.2 Hz.

5. Conclusion

In this work, we have demonstrated a dual wavelength band single-pixel telescope system, capable of performing real-time VIS and SWIR imaging simultaneously. At 64×64 pixel resolution, our system achieved continuous VIS and SWIR imaging at a frame rate of 2.4 Hz which we applied to imaging in various weather conditions. In contrast to conventional multispectral imaging systems, we are able to provide perfect pixel registration between the images. Our single-pixel telescope system provides an alternative cost-effective method for multispectral imaging applications.

The data used to produce the results presented in this manuscript is available at http://dx.doi.org/10.5525/gla.researchdata.1015

Funding

QuantIC (EP/M01326X/1); European Research Council (340507).

Acknowledgments

The authors thank Krzysztof Konrad Brzozowski, Kyle Nutt and Jakub Bělín for assisting the outdoor transportation.

Optics EXPRESS

Disclosures

The authors declare no conflicts of interest.

References

1. M. F. Duarte, M. A. Davenport, D. Takhar, J. N. Laska, T. Sun, K. Kelly, and R. G. Baraniuk, "Single-pixel imaging via compressive sampling," IEEE Signal Process. Mag. **25**(2), 83–91 (2008).
2. W. L. Chan, K. Charan, D. Takhar, K. F. Kelly, R. G. Baraniuk, and D. M. Mittleman, "A single-pixel terahertz imaging system based on compressed sensing," Appl. Phys. Lett. **93**(12), 121105 (2008).
3. Y. Bromberg, O. Katz, and S. Silberberg, "Ghost imaging with a single detector," Phys. Rev. A **79**(5), 053840 (2009).
4. J. Ma, "Single-pixel remote sensing," IEEE Trans. Geosci. Remote Sens. Lett. **6**(2), 199–203 (2009).
5. Z. Zhang, X. Ma, and J. Zhong, "Single-pixel imaging by means of Fourier spectrum acquisition," Nat. Commun. **6**(1), 6225 (2015).
6. M. P. Edgar, G. M. Gibson, and M. J. Padgett, "Principles and prospects for single-pixel imaging," Nat. Photonics **13**(1), 13–20 (2019).
7. P. A. Morris, R. S. Aspden, J. E. C. Bell, R. W. Boyd, and M. J. Padgett, "Imaging with a small number of photons," Nat. Commun. **6**(1), 5913 (2015).
8. D. Shin, F. Xu, D. Venkatraman, R. Lussana, F. Villa, F. Zappa, V. K. Goyal, F. N. C. Wong, and J. H. Shapiro, "Photon-efficient imaging with a single-photon camera," Nat. Commun. **7**(1), 12046 (2016).
9. G. A. Howland and J. C. Howell, "Efficient high-dimensional entanglement imaging with a compressive-sensing double-pixel camera," Phys. Rev. X **3**(1), 011013 (2013).
10. G. A. Howland, S. H. Knarr, J. Schneeloch, D. J. Lum, and J. C. Howell, "Compressively characterizing high-dimensional entangled states with complementary, random filtering," Phys. Rev. X **6**(2), 021018 (2016).
11. B. Sun, M. P. Edgar, R. Bowman, L. E. Vittert, S. Welsh, A. Bowman, and M. Padgett, "3D computational imaging with single-pixel detectors," Science **340**(6134), 844–847 (2013).
12. Y. Zhang, M. P. Edgar, B. Sun, N. Radwell, G. M. Gibson, and M. J. Padgett, "3D single-pixel video," J. Opt. **18**(3), 035203 (2016).
13. M.-J. Sun, M. P. Edgar, G. M. Gibson, B. Sun, N. Radwell, R. Lamb, and M. J. Padgett, "Single-pixel three-dimensional imaging with time-based depth resolution," Nat. Commun. **7**(1), 12010 (2016).
14. D. Shrekenhamer, C. M. Watts, and W. J. Padilla, "Terahertz single pixel imaging with an optically controlled dynamic spatial light modulator," Opt. Express **21**(10), 12507–12518 (2013).
15. C. M. Watts, D. Shrekenhamer, J. Montoya, G. Lipworth, J. Hunt, T. Sleasman, S. Krishna, D. R. Smith, and W. J. Padilla, "Terahertz compressive imaging with metamaterial spatial light modulators," Nat. Photonics **8**(8), 605–609 (2014).
16. R. I. Stantchev, B. Sun, S. M. Hornett, P. A. Hobson, G. M. Gibson, M. J. Padgett, and E. Hendry, "Noninvasive, near-field terahertz imaging of hidden objects using a single-pixel detector," Sci. Adv. **2**(6), e1600190 (2016).
17. N. Radwell, K. J. Mitchell, G. M. Gibson, M. P. Edgar, R. W. Bowman, and M. J. Padgett, "Single-pixel infrared and visible microscope," Optica **1**(5), 285–289 (2014).
18. M. P. Edgar, G. M. Gibson, R. W. Bowman, B. Sun, N. Radwell, K. J. Mitchell, S. S. Welsh, and M. J. Padgett, "Simultaneous real-time visible and infrared video with single-pixel detectors," Sci. Rep. **5**(1), 10669 (2015).
19. K. Fan, J. Y. Suen, and W. J. Padilla, "Graphene metamaterial spatial light modulator for infrared single pixel imaging," Opt. Express **25**(21), 25318–25325 (2017).
20. G. M. Gibson, B. Sun, M. P. Edgar, D. B. Phillips, N. Hempler, G. T. Maker, G. P. Malcolm, and M. J. Padgett, "Real-time imaging of methane gas leaks using a single-pixel camera," Opt. Express **25**(4), 2998–3005 (2017).
21. W.-K. Yu, X.-F. Liu, X.-R. Yao, C. Wang, Y. Zhai, and G.-J. Zhai, "Complementary compressive imaging for the telescopic system," Sci. Rep. **4**(1), 5834 (2015).
22. M.-J. Sun and J.-M. Zhang, "Single-pixel imaging and its application in three-dimensional reconstruction: A brief review," Sensors **19**(3), 732 (2019).
23. Y. Zhang, "Investigations into applications of photometric stereo and single-pixel imaging," PhD diss., University of Glasgow, 51-52 (2017).
24. Y. A. Geadah and M. J. G. Corinthios, "Natural, dyadic, and sequency order algorithms and processors for the Walsh-Hadamard transform," IEEE Trans. Comput. **C-26**(5), 435–442 (1977).
25. M. Corinthios, *Signals, Systems, Transforms, and Digital Signal Processing with MATLAB* (CRC Press, 2009).
26. L. Wang and S. Zhao, "Fast reconstructed and high-quality ghost imaging with fast Walsh-Hadamard transform," Photonics Res. **4**(6), 240–244 (2016).
27. J. Westfall and S. William, "The Lunar Eclipse Experience," *Celestial Shadows*, Springer NY, 75–95 (2015).
28. S. D. Johnson, D. B. Phillips, Z. Ma, S. Ramachandran, and M. J. Padgett, "A light-in-flight single-pixel camera for use in the visible and short-wave infrared," Opt. Express **27**(7), 9829–9837 (2019).